
This is an electronic reprint of the original article.
This reprint may differ from the original in pagination and typographic detail.

Meles, Mehari; Rajasekaran, Akash; Menta, Estifanos; Mela, Lauri; Jäntti, Riku
Impact of hardware impairments and BS antenna tilt on 3D drone localization and tracking

Published in:
Aeu International Journal of Electronics and Communication

DOI:
[10.1016/j.aeue.2024.155543](https://doi.org/10.1016/j.aeue.2024.155543)

Published: 01/12/2024

Document Version
Publisher's PDF, also known as Version of record

Published under the following license:
CC BY

Please cite the original version:
Meles, M., Rajasekaran, A., Menta, E., Mela, L., & Jäntti, R. (2024). Impact of hardware impairments and BS antenna tilt on 3D drone localization and tracking. *Aeu International Journal of Electronics and Communication*, 187, Article 155543. <https://doi.org/10.1016/j.aeue.2024.155543>

This material is protected by copyright and other intellectual property rights, and duplication or sale of all or part of any of the repository collections is not permitted, except that material may be duplicated by you for your research use or educational purposes in electronic or print form. You must obtain permission for any other use. Electronic or print copies may not be offered, whether for sale or otherwise to anyone who is not an authorised user.



Impact of hardware impairments and BS antenna tilt on 3D drone localization and tracking

Mehari Meles*, Akash Rajasekaran, Estifanos Yohannes Menta, Lauri Mela, Riku Jäntti

Department of Information and Communications Engineering, Aalto University, Espoo, 02150, Uusimaa, Finland

ARTICLE INFO

Keywords:

CFO
PN
MUSIC
AOA
EKF
LS

ABSTRACT

Today, GPS-free drone localization is increasingly gaining attention in various applications, but it faces significant accuracy challenges in three-dimensional (3D) space due to various impairments. This study investigates the effects of carrier frequency offset (CFO), phase noise (PN), and down-tilted base station (BS) antennas on drone positioning and tracking. Additionally, we explore the impact of inter-site distance (ISD) and BS density on drone position estimation accuracy. In our methodology, we consider a flying drone equipped with a single transmission antenna and BSs configured with 4×4 antennas under specific impairments. We first analyze the effects of these impairments on the signal's covariance matrix. Then, using the MUSIC algorithm, we estimate the azimuth and elevation angles, which serve as the basis for drone localization using the Least Squares (LS) method across all BSs. Finally, the estimated positions feed into an Extended Kalman Filter (EKF) for tracking. Our results present a sequential analysis of the impact of all impairments on the off-diagonal covariance matrix, on the Angle of Arrival (AOA) estimation and 3D drone localization. We use simulations to demonstrate how hardware impairments affect 3D drone localization accuracy under varying ISD and BS densities.

1. Introduction

Accurately localizing a drone is a critical requirement for ensuring safe and efficient operations for several applications. Traditionally, Global Positioning System (GPS) has served as a prominent method for the localization of aerial vehicles, including airplanes [1]. Relying only on GPS can result in localization failures, particularly when the transmitter and receiver are not in direct line of sight (LoS). The topic of network-based drone localization has been active research for several years. However, it has numerous challenges within GPS-free aeronautical positioning systems requiring substantial efforts to improve accuracy. Some of the challenges for network based localization are sensor errors, signal multipath, and integration complexity, which necessitate complex data fusion and frequent system calibration. Besides, dependency on external infrastructure, and increased vulnerability to interference, impacting their accuracy and reliability.

Numerous techniques have been introduced to enhance the precision of 3D UAV (Unmanned Aerial Vehicle) localization. To enhance the positioning accuracy of unmanned aerial vehicles (UAVs), a new approach is proposed that utilizes multiple received signal strength (RSS) measurements from various base station (BS) receiver and multiple points along a defined trajectory path [2]. The process begins by fixing one of the BSs and conducting multiple measurements along the defined

trajectory. Subsequently, the location of the UAV is estimated using the Maximum Likelihood (ML) technique. Similarly, the calculated UAV locations from all participating BSs are combined to estimate the position of the UAV. However, high-speed movement of the UAV can introduce Doppler shifts, a result of its relative motion to the BS transmitters. Such frequency offsets can reduce the location estimation accuracy, which the authors did not consider.

The challenges associated with the performance and complexity of network-based drone localization have gained significant research interest. Studies in [3] & [4], have explored the utilization of cascading CAPON and Beamspace Multiple Signal Classification (MUSIC) for direction estimation. However, Angle of Arrival (AOA) estimation still faces difficulties, especially when the UAV experiences fast dynamic states during hovering. Receiver carrier frequency offset (CFO) is a common occurrence in communication systems and this can impact position estimation accuracy. The research presented in [5], has primarily focused on investigating the effects of CFO on AOA based estimation for Bluetooth Low Energy (BLE) location estimation. Additionally, the authors derived the Cramer–Rao bound (CRB) to assess accuracy estimation. Although the research is compelling and has been validated in both experimental and simulation, its application to 3D estimation performance remains unexplored.

* Corresponding author.

E-mail address: mehari.meles@aalto.fi (M. Meles).

Literature in [6] have explored the use of The Estimation of Signal Parameters via Rotational Invariance Techniques (ESPRIT) for estimating AOA by leveraging the synthetic ESPRIT algorithm and applying it to Code Division Multiple Access (CDMA) signals. To address the challenge of the size of antenna array in data collection for ESPRIT-based estimations, the authors introduced a synthesis technique. This method enabled the antennas to locate in flexible positions, which solve the constraints of the actual antenna array sizes.

Researchers in [7] discussed UAV detection and positioning built on multi-dimensional signal, which is executed in two stages. The initial step involves monitoring the communication channel between the UAV and its controller. For detection, machine learning algorithms were employed, integrating wavelet energy entropy (WEE), signal frequency spectrum (SFS), and power spectral entropy (PSE) to extract information. Once the UAV is identified, it is localized using the azimuth angle and elevation angle. The study also compared the precision of two dimensional (2D) and 3D location estimations over short distances.

The work in [8] presents a method for 2D Direction of Arrival (DOA) estimation for incoherently distributed signal sources using Uniform Rectangular Arrays (URA). They introduce an estimation technique for 2D incoherent distributed sources and employ the ESPRIT algorithm. Through simulations, they analyze the efficiency of their proposed method, especially in contexts involving sources with varying angular power density functions, sensor distances, and boundary region sources. Their investigations range with different scenarios, including varying Signal to Noise Ratio (SNR), angular power density functions, sensor distances, and the number of sources. Considerably, their technique proves capable of estimating a higher number of sources when given an adequate number of sources, especially when using large dimensional arrays.

Based on specific application needs, extensive research has been conducted on UAV communication networks, focusing on UAV-to-ground and direct UAV-to-UAV communications. To ensure optimal coverage for ground users, local BSs are typically downtilted. Research has been done in [9] to assess the effects of downtilting BSs on ultra-dense networks (UDNs) performance. To accomplish this, they employ a two-step approach: initially, they model the channel between an elevated BS and a ground user as a 3-D line-of-sight channel, considering the effect of the height of the BSs. The communication between UAV and ground is modeled by considering height of the UAV and the corresponding path loss [10].

To address the constraints in GPS-free localization, numerous studies have explored the integration of various methods. One study in [11] introduced an innovative approach to localize targets using a combination of RSS and AOA measurements. This technique employs approximated error covariance matrix for a weighted least squares (WLS) solution that does not require the prior ground truth locations or noise variance estimations. Simulation validations demonstrate its superior performance. Multiple methods have been employed in localizing the mobile aerial transmitters. Many well-known passive localization methods are based on the Time Difference Direction of Arrival (TDOA) and AOA of the signals at the BSs receivers as studied in [12] & [13]. In the paper [14], a model is presented that localizes aerial transmitters in Line-of-Sight (LoS) communication using two TDOA-based methods and one AOA-based method. The study further examines the impact of various BS topologies and the number of required BSs on localization accuracy.

BS transceivers are typically down-tilted to serve terrestrial users effectively. Contrary to this, BSs intended for aerial vehicles require specific adjustments. Research [15] suggests that antennas need to be up tilted to optimally serve aerial vehicles through the main beam. The study provides approximate expressions for Signal-to-Interference Ratio (SIR)-based coverage probabilities for both aerial and ground users.

In our previous paper [16], we equipped the drone with two antenna elements to measure the signals from multiple BSs. Using this setup, the drone estimates the AOA by mechanically rotating the two

antenna elements. After estimating the AOA from various BSs, the location of the drone is determined on a 2D plane utilizing the LS algorithm. We evaluated the method in scenarios where the drone is both stationary and hovering and subsequently compared the results. In our follow up study [17] & [18], we explored drone positioning and tracking through measurements using a drone fitted with a single antenna for signal transmission and two 4X4 URA receivers for signal reception. The drone was flown in zigzag and up-and-down patterns, covering a distance of less than 25 meters. For positioning and tracking, we employed the MUSIC and Extended Kalman Filter (EKF) methods, respectively.

1.1. Main contribution

In this paper, we conduct simulations on network-based drone localization and tracking, focusing on evaluating localization accuracy under various impairments, such as phase noise (PN), CFO, ISD, the number of BSs in the coverage area and BS tilting. Our key contributions are summarized as follows:

- By maintaining constant spacing of the antenna elements in the URA, we model and analyze the impact of impairments on the 3D steering vector of the arrays.
- Analysis and modeling the effect of impairments on the covariance matrix.
- Analysis the impairments on AOA estimation using the MUSIC algorithm, location using LS method for every snapshot over all participating BSs for the positioning.
- Modeling drone localization and tracking with impairments.
- BS antennas are typically downtilted, which impacts AOA-based localization. Our study assesses how downtilt angles influence the accuracy of drone location estimation.
- We conducted a comparative analysis to evaluate the influence of number of BS receiver and ISD on positioning accuracy in both 2D and 3D space.
- We validated our angle estimation approach against the theoretical performance bound by employing the Cramér-Rao Lower Bound (CRLB), which serves as a benchmark for the minimum variance an unbiased estimator can achieve.

1.2. Organization of the paper

The structure of the paper is organized as follows. Section 2 gives the system model and phases of the localization system. Section 3 briefly describes the methodology used for positioning and tracking. Section 4 presents the simulation setup and analytical results. Lastly, Section 5 concludes the paper.

2. System modeling

In this section, we present an overview of the system model used for drone positioning and tracking. We consider, as shown in Fig. 1, a hexagonal cellular layout with B BSs.

Each BS, located at the center of its respective cell, is equipped with an $M = M_y \times M_z$ linear antenna array receiver. All BS receivers are positioned in a known location ensuring a direct line of sight communication with the drone, and every BS collects n samples.

In this paper, we propose the array configuration shown in Fig. 2(a), incorporating a $\frac{\lambda}{4}$ shift of the antenna elements along the y -axis. This adjustment ensures unobstructed LOS visibility for the drone across all antenna elements, preventing potential obstructions that could complicate the estimation process. Without this shift, the antenna elements could obstruct each other and block the LOS to the drone, thereby complicating the estimation process. We evaluated the accuracy improvement of 3D drone location estimation by comparing results from the shifted configuration against those from an unshifted configuration

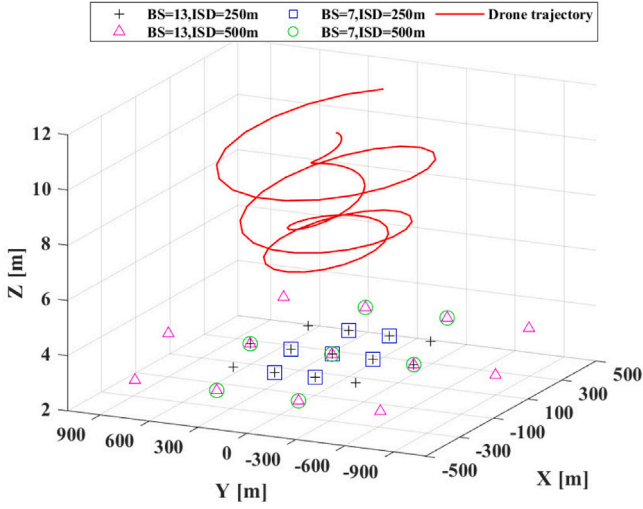
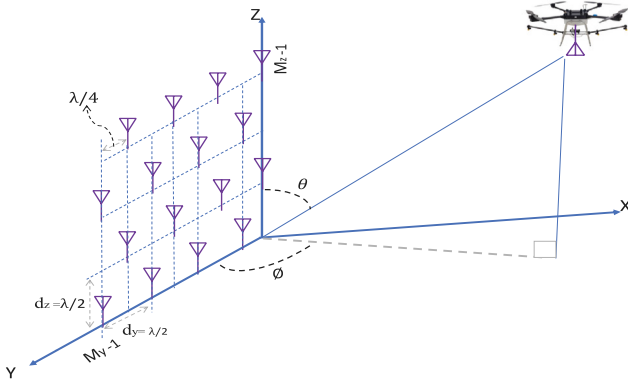
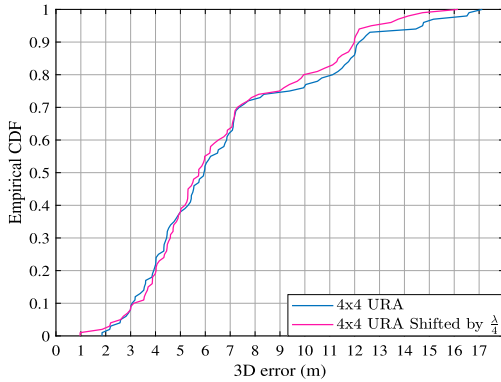


Fig. 1. Model of the drone trajectory path and known position information of BS layout.



(a)



(b)

Fig. 2. Array configuration:(a) the 4×4 URA antenna employed in this study. (b) Comparison the estimation accuracy of the array when it is shifted by $\lambda/4$ versus without any shift.

as shown in Fig. 2(b). In both scenarios, the BS location remained unchanged, with adjustments made only to the positions of its elements. We chose to utilize this antenna array in our simulation study as it aligns with the array employed in our previous measurements [17,18].

2.1. System design

The system flow diagram presented in Fig. 3 outlines the process of signal modeling, drone positioning and tracking. The drone, equipped with a single transmitting antenna, follows a predefined spiral trajectory. BS receivers capture the signal emanating from the drone. However, this signal is often affected by CFO and PN impairments, which can challenge the localization process. In this paper, we employ the MUSIC algorithm for drone position estimation. Subsequently, using the estimated 3D AOA from all the BSs, we apply the least squares techniques to precisely estimate the location of the drone in 3D plane. EKF is applied to track the trajectory of the drone movement over time. The model process, from signal processing, positioning, and tracking, is represented in Fig. 3.

3. Proposed methodology

Once the system has been modeled, the next phase involves the parameter estimation of the 3D position of the drone. This section will provide the model and methodology employed for the impact of the impairments on drone positioning and tracking.

3.1. Signal model

Consider S as the transmitted signal from the drone, and the received signal at the i th BS can be described by the following model:

$$\mathbf{y}_i(k) = F_i(k)\mathbf{a}_i(\theta_{ik}, \phi_{ik})S(k) + \mathbf{n}_i(k), \quad (1)$$

where $\mathbf{y}_i(k)$ is the received signal vector at the i th BS for the time step k . $F_i(k)$ is a matrix that models the impact of the phase CFO and PN, which can be given as:

$$F_i(k) = \text{diag} (e^{j(w_{\ell}k + \psi_{\ell}k)}), \quad (2)$$

where $w_{\ell} \sim \mathcal{U}(-W_m, W_m)$ is a uniformly distributed random variable modeling the CFO, and $\psi_{\ell} \sim \mathcal{N}(0, \sigma_{\psi}^2)$ is a Gaussian distributed random variable modeling the PN, both at the ℓ th antenna element. The array response vector of the i th BS receiver, denoted by $\mathbf{a}_i(\theta_{ik}, \phi_{ik})$, is associated with the AOA angles θ_{ik} and ϕ_{ik} . $S(k)$ denotes the transmitted signal vector at time k , while $\mathbf{n}_i(k)$ represents the additive noise vector at the i th BS at time k . As shown in Fig. 2(a), the antenna elements are positioned in $y - z$ plane. Using the y -axis rotation matrix in [19], we down tilt the antenna elements.

3.2. Impact of impairments on covariance matrix

Here, before we estimate the 3D AOA at each of the BS receivers given in Fig. 1, we will analyze the impact of the impairments on the covariance. The estimation of the 3D AOA involves the computation of the covariance matrix of the received signal (1):

$$R_{yy,i}(k) = \frac{1}{n} \sum_{k=1}^n \mathbf{y}_i(k)(kT_s)\mathbf{y}_i(k)^H(kT_s), \quad (3)$$

where H and T_s are Hermitian transpose and sampling time, respectively. The AOA estimation relies on the coherence and consistency of the signals received across the antennas.

In this paper, we analyze a scenario where a drone transmits a set of $n = 20$ samples. To evaluate the signal characteristics from these transmissions, we compute the covariance matrix by taking the average of the sample set. An accurate covariance matrix relies on precise phase information to determine how the signal power is distributed across different directions. Phase errors can lead to an incorrect assessment of signal coherence and correlation, impacting the ability to distinguish between signals from different directions. In the MUSIC algorithm, the diagonal elements of the covariance matrix represent the power of the signals received at each antenna element, while the off-diagonal

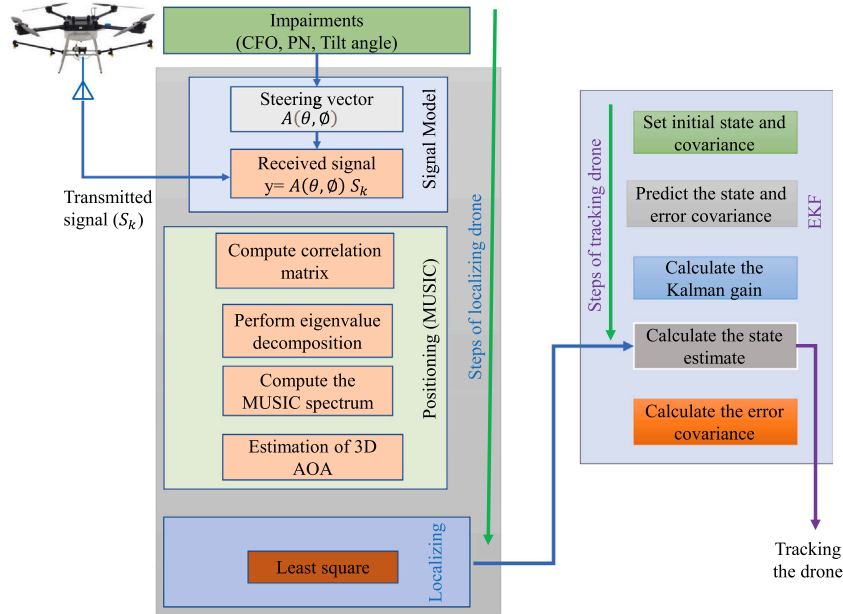


Fig. 3. Considered system flow diagram.

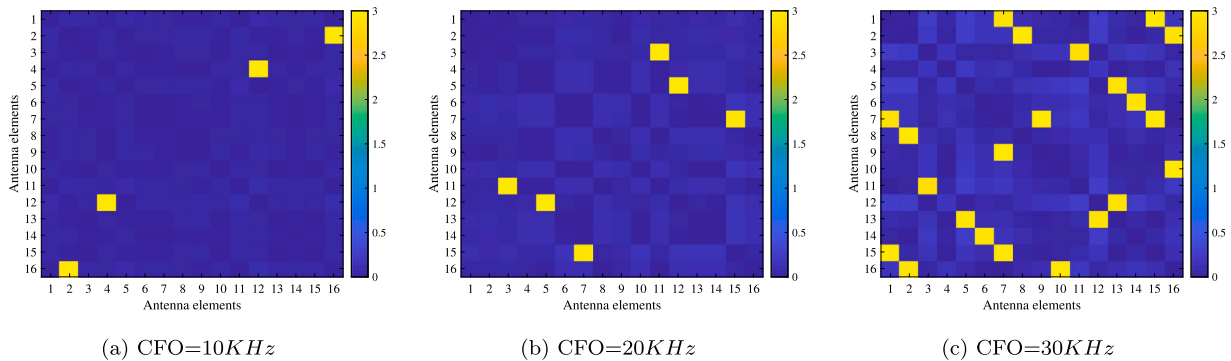


Fig. 4. Phase error (radians) of the off-diagonal elements under various CFO.

elements indicate the correlation between signals received at different antenna elements. Accurate AOA estimation are achieved when the covariance matrix effectively captures the correlation structure (off-diagonal elements) of the incoming signals across the antenna array.

The off-diagonal elements are critical for precise AOA estimations as they provide essential information about the relative phases between signals arriving at each antenna. Impairments in the antenna elements can significantly degrade the performance of the MUSIC algorithm. Figs. 4, 5, and 6 demonstrate the impact of CFO, PN, and down tilt on phase accuracy, respectively. As shown, increasing impairment values lead to a rise in phase error in the off-diagonal elements, which distorts the covariance matrix. This distortion subsequently causes inaccuracies in AOA estimation, as direction-finding algorithms rely on an accurate covariance matrix.

Referring to Figs. 4(a), 4(b), and 4(c), it is evident that the phase error associated with the off-diagonal matrix increases with CFO increments—from 10 kHz to 20 kHz, and up to 30 kHz. This demonstrates how the phase error escalates as the CFO impairment increases.

Similarly, Figs. 5(a), 5(b), and 5(c) illustrate how the received signal, when rotated due to PN introduced at each antenna element,

causes the off-diagonal elements of the covariance matrix to deviate from the ideal case without impairments. Additionally, these figures demonstrate that the phase error in the off-diagonal elements increases as the PN rises.

Unlike PN and CFO, which require a Gaussian random variable to apply different impairments to each antenna element, BS downtilt only slightly alters the positions of the antenna elements, resulting in a lesser impact on the off-diagonal elements of the covariance matrix.

As a result, its effect on AOA is less significant compared to PN and CFO. The impact of BS downtilt is given in Fig. 6(a), 6(b), and 6(c), which show small increments in phase error.

3.3. Impact of impairments on AOA estimation

To accurately determine the 3D coordinates of the drone, accurate estimation of both angle of azimuth and elevation is essential. For this purposes, researchers have commonly employed the MUSIC algorithm, as outlined in [20] & [21]. However, the MUSIC algorithm have its drawbacks as it involves the computation of eigenvectors from correlation matrices, which can become computationally intensive, particularly computing large matrix dimensions.

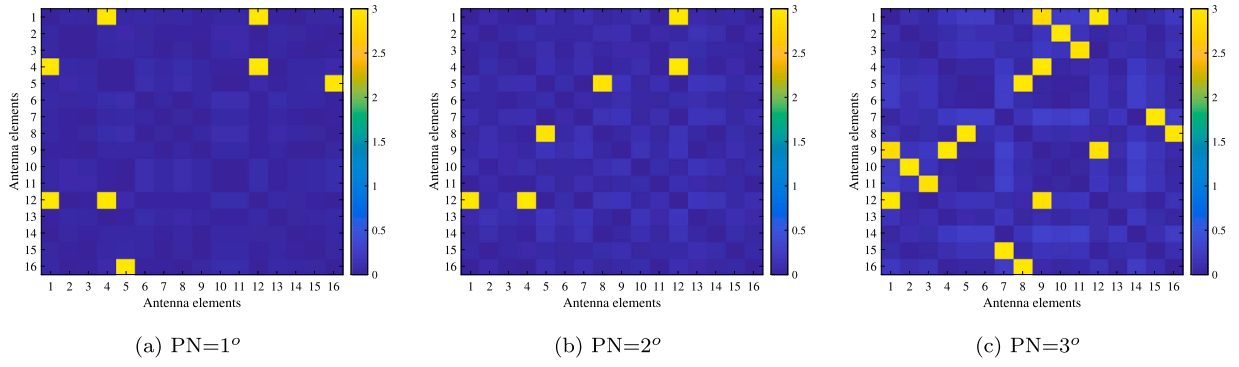


Fig. 5. Phase error (radians) of the off-diagonal elements under various PN.

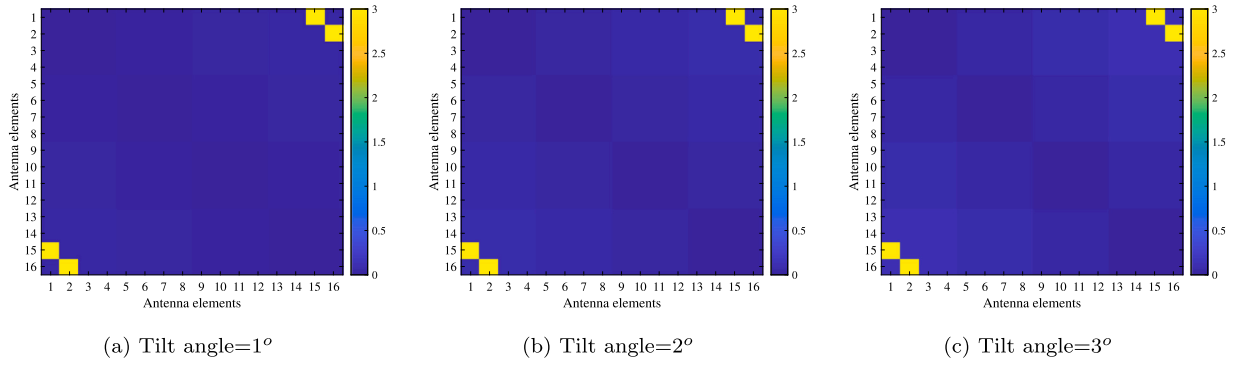


Fig. 6. Phase error (radians) of the off-diagonal elements under various tilt angles.

Considering from the derivations presented in [20] & [7], MUSIC algorithm focuses on estimating the noise subspace of the correlation matrix given in (3). This process entails performing an eigenvalue decomposition (EVD) and selecting the eigenvectors corresponding to the K smallest eigenvalues. The noise subspace matrix is then represented as $\mathbf{E}_i = [\mathbf{e}_{K+1}, \dots, \mathbf{e}_M]$, where M represents the number of antenna elements in the BS receiver. Following the derivation [7], the azimuth and elevation are estimated by identifying maximum peak values in the spectrum $P(\theta, \phi)$ of the covariance matrix:

$$P_i(\theta_{ik}, \phi_{ik}) = \frac{1}{\mathbf{a}_i^H(\theta_{ik}, \phi_{ik}) \mathbf{E}_i \mathbf{E}_i^H \mathbf{a}_i(\theta_{ik}, \phi_{ik})}, \quad (4)$$

where $\mathbf{a}_i(\theta_{ik}, \phi_{ik})$ represents the response vector for the i th BS receiver at the k sampling time, while \mathbf{E}_i corresponds to the noise subspace matrix obtained through the eigenvalue decomposition of the correlation matrix.

The AOA estimation solely depends on the accuracy of the off diagonal covariance matrix. In this work, we explore the effects of various impairments on azimuth and elevation error estimations. Figs. 7 and 8 illustrate that increased impairments lead to rise in angle variance, which refers to the extent to which the angle estimations deviate from the mean angle. A higher variance indicates that the angle estimations are more spread out around the mean, indicating greater uncertainty in angle estimations. Specifically, as observed in Fig. 7, the presence of three distinct impairments contributes to the error in azimuth estimation.

Once the off-diagonal elements of the covariance matrix are impacted by the impairments, as shown in Figs. 7(a), 7(b), and 7(c), the resulting phase errors lead to uncertainty in AOA estimations. Overall, as demonstrated in Fig. 7, with higher impairments, the variance of the azimuth error estimation worsen. Fig. 8 demonstrates that as impairment values rise, like that of in azimuth, there is a slight increase in error estimation for the elevation angle. Table 1 presents the mean errors for both azimuth and elevation.

3.4. CRLB analysis for AoA estimation

The channel parameter estimation state-vector at the i th BS at time-instant k , denoted by $\zeta_{ik} \in \mathbb{R}^2$, can be given as:

$$\zeta_{ik} = [\phi_{ik} \quad \theta_{ik}]^T. \quad (5)$$

Given the signal model, the general deterministic CRLB on the covariance matrix of unbiased channel parameter estimator of ζ is stated in [22]:

$$\text{CRLB}_\zeta = \frac{\sigma_w^2}{2} \{ \Re \{ \mathbf{S}^\dagger \mathbf{D}^\dagger \Pi_A^\perp \mathbf{D} \mathbf{S} \} \}^{-1}, \quad (6)$$

where σ_w^2 the noise variance, \mathbf{S} denotes a diagonal matrix that contain the transmitted signal, Π_A^\perp represent the projection onto nullspace of A given as $\Pi_A^\perp = \mathbf{I} - \mathbf{A}(\mathbf{A}^\dagger \mathbf{A})^{-1} \mathbf{A}^\dagger$, where A is the beampattern of m far-field sources, and \dagger denote the conjugate transpose. \mathbf{D} is the partial derivative of A with respect to ζ :

$$\mathbf{A} = [a(\phi_1, \theta_1), a(\phi_2, \theta_2), \dots, a(\phi_m, \theta_m)] \quad (7a)$$

$$\mathbf{D} = [a'_1, a'_2, \dots, a'_m], a'_m = \frac{\partial a_m}{\partial \zeta_m}. \quad (7b)$$

Fig. 9 shows the AOA estimation performance for one BS in the presence of impairments, showing that the variance of the azimuth and elevation estimations is close to the CRLB, indicating an efficient estimator. It should be noted that the level of closeness between the CRLB and the variance varies depending on the BS position. For visualization purposes, we considered a single BS, so the observed closeness may not apply to other BSSs. From the CRLB plot, the azimuth angle is close to 10^{-5} degrees, while the variance under impairments fluctuates between 10^{-2} and 10^{-1} degrees. Similarly, for the elevation angle, the CRLB is mostly within 10^{-7} degrees, with the variance also ranging from 10^{-2} to 10^{-1} degrees. The magnitude of closeness, calculated as the logarithm of the ratio between the variance and the CRLB, is nearly 3

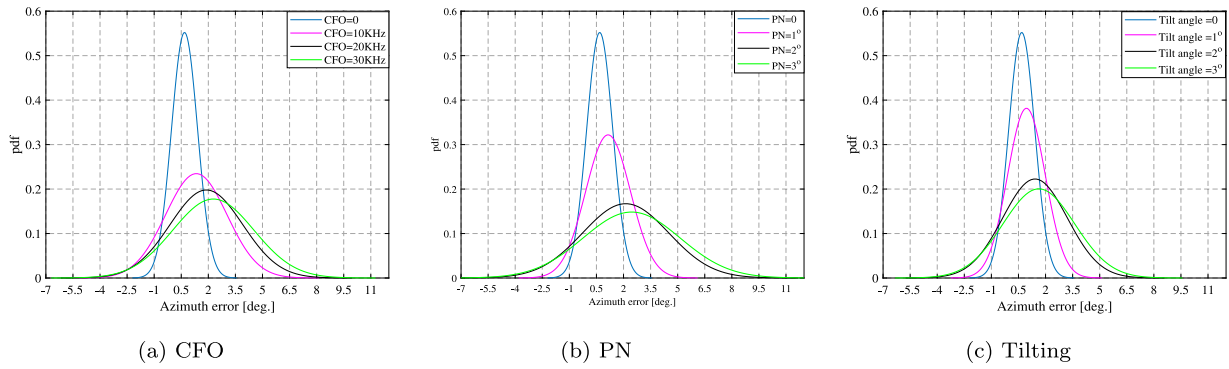


Fig. 7. Impacts of the impairments on Azimuth considering the BS at the center of Fig. 1.

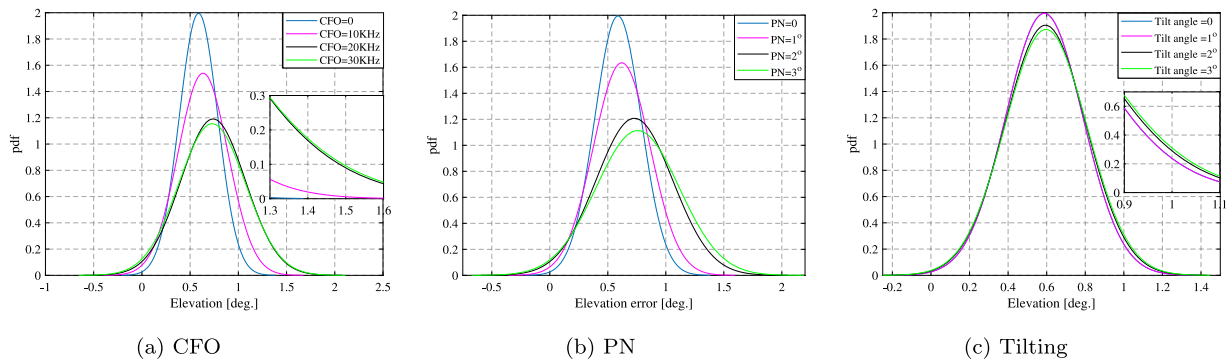


Fig. 8. Impacts of the impairments on Elevation considering the BS at the center of Fig. 1.

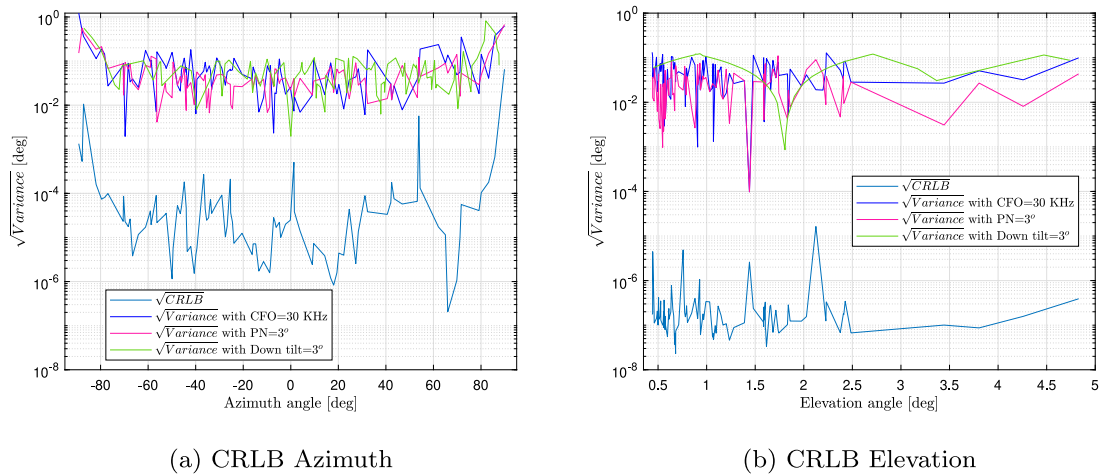


Fig. 9. CRLB vs estimated variance of angles using MUSIC based on the technical impairments.

Table 1
Mean AOA error estimation.

Error	CFO				PN				Tilting angle			
	0 KHz	10 KHz	20 KHz	30 KHz	0°	1°	2°	3°	0°	1°	2°	3°
Azimuth (°)	0.65	1.26	1.8	2.4	0.65	1.2	2	2.8	0.65	1	1.5	1.7
Elevation (°)	0.55	0.65	0.75	0.78	0.6	0.65	0.75	0.85	0.58	0.6	0.63	0.65

to 4 orders of magnitude:

$$\text{Magnitude of Closeness} = \log_{10} \left(\frac{\text{Variance}}{\text{CRLB}} \right) \approx 3 \text{ to } 4 \quad (8)$$

While the variance is not as tight as the CRLB, it remains relatively close in terms of orders of magnitude. Similarly, the magnitude of closeness of the elevation is approximately 5 to 6.

3.5. Impact of number of available BS and ISD on positioning accuracy

Since 3D positioning is dependent on AOA, any inconsistencies on the covariance and angles impacts positioning. Additionally, factors such as ISD and the number of BS receivers play a critical role in determining positioning accuracy.

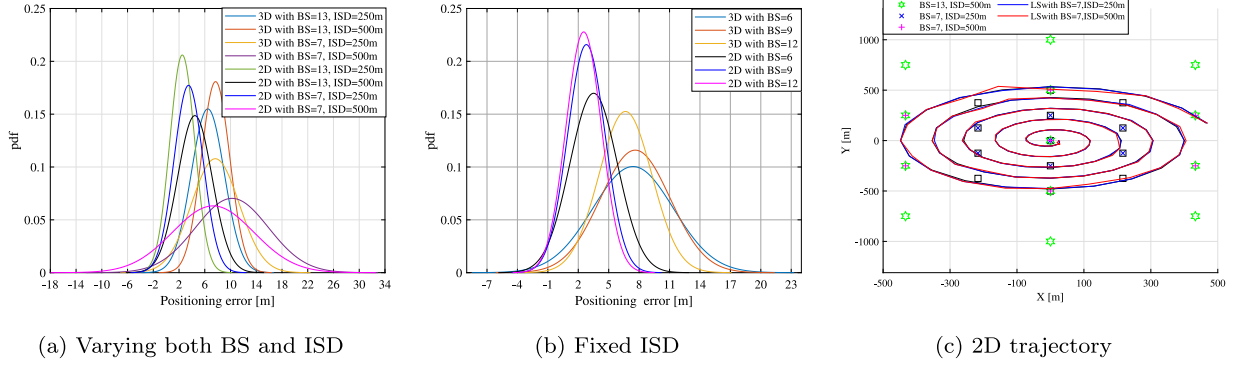


Fig. 10. Location estimation performance with respect to number of BS and ISD without the impairments.

To examine the effects of ISD and the density of participating BS receivers on positioning accuracy, we initially set a defined area with a fixed spiral trajectory. We then varied both the ISD and the number of BS.

Additionally, careful design consideration for the number of BSs, ISD, and trajectory is crucial, as simply increasing the number of BSs does not necessarily yield significant improvements in drone location accuracy, as seen in Figs. 10. To determine the optimum number of BS, we need to consider the area of interest, the type of antennas used, and the number of antennas utilized in both the transmitter and receiver.

Figs. 10(a) and 10(b) compare the distribution of positioning errors in 2D and 3D localization systems under different configurations, by varying the number of BS and ISD. Fig. 10(a) shows location accuracy in 2D and 3D as a function of BS count and ISD. Generally, it can be observed that more BSs and smaller ISDs result in better positioning accuracy. Fig. 10(b) presents the localization error distribution for different numbers of BS while keeping ISD constant. Overall, Figs. 10(a) and 10(b) illustrate that increasing the number of BSs tends to enhance localization accuracy in both 2D and 3D configurations. Fig. 10(c) presents the overall configuration and results of a simulation aimed at assessing the accuracy of 2D location estimations. It depicts the true spiral trajectory and the estimated 2D positions using 7 BS with ISDs of 250 meters and 500 meters. The plot shows the position of set of BSs and the accuracy of the location estimations compared to the true trajectory in the 2D plane.

3.6. Drone location estimation

Let us assume that we have a set of BSs B with known coordinates (x_i, y_i, z_i) and corresponding elevation and azimuth angles (θ_i, ϕ_i) for each BS. To estimate the location of the drone using the least square method, with the following steps:

$$\mathbf{d}_i = [\cos(\phi_i) \cos(\theta_i) \quad \cos(\phi_i) \sin(\theta_i) \quad \sin(\phi_i)], \quad (9)$$

where \mathbf{d}_i is the direction vector for the i th line in space. The equation for the line from BS i towards the drone can then be represented as:

$$\mathbf{r}_i(t) = [x_i \quad y_i \quad z_i]^T + t_i \cdot \mathbf{d}_i, \quad (10)$$

where t_i is a scalar that extends along the direction vector, and \cdot denotes the dot product.

The goal is to find a point $\mathbf{P} = [X \quad Y \quad Z]^T$ in space that minimizes the distances to each of the lines. This translates to solving the following optimization problem:

$$\min_{X,Y,Z} \sum_{i=1}^B \|(\mathbf{P} - \mathbf{r}_i(t_i)) \times \mathbf{d}_i\|^2, \quad (11)$$

where \times denotes the cross product and B is the number of BSs. The coordinates (x, y, z) gives the estimated location of the drone based on the 3D AOA estimation over all BSs.

3.7. Drone trajectory tracking

Once the drone is positioned in 3D plane based on the above sections, the next phase is tracking the drone. In this paper, we utilized the EKF algorithm, which linearizes the nonlinear model based on the current mean and covariance through a first-order Taylor series. As detailed in [23] & [24], the linearized variant of the nonlinear state is used for estimation of the state via EKF algorithm. Let the state of the drone be represented as:

$$\mathbf{x} = [x \quad y \quad z \quad \dot{x} \quad \dot{y} \quad \dot{z}]^T, \quad (12)$$

where (x, y, z) and $(\dot{x}, \dot{y}, \dot{z})$ are the 3D position and velocity components, respectively. The process model predicts the next state based on the current state and control inputs:

$$\mathbf{x}_{k+1} = f(\mathbf{x}_k, \mathbf{u}_k) + \mathbf{w}_k, \quad (13)$$

where f is the nonlinear state transition function and \mathbf{u}_k is the control input vector, and \mathbf{w}_k is the process noise.

The measurement model relates the true state of the trajectory of the drone to the measurements that are observed:

$$\mathbf{z}_k = h(\mathbf{x}_k) + \mathbf{v}_k, \quad (14)$$

where h is the nonlinear measurement function, and \mathbf{v}_k is the measurement noise.

The EKF linearizes the process and measurement models using a first-order Taylor expansion about the current estimate:

$$F_k = \left. \frac{\partial f}{\partial \mathbf{x}} \right|_{\mathbf{x}=\hat{\mathbf{x}}_k}, \quad H_k = \left. \frac{\partial h}{\partial \mathbf{x}} \right|_{\mathbf{x}=\hat{\mathbf{x}}_k}, \quad (15)$$

where F_k and H_k are the Jacobian matrix of the process and measurement models, respectively. The EKF algorithm has two stages.

Prediction step

Let $\hat{\mathbf{x}}_{k|k-1}$ be the predicted state estimate at time step k based on the previous estimate $\hat{\mathbf{x}}_{k-1|k-1}$ and control input u_k , and let $P_{k|k-1}$ be the predicted error covariance matrix. Then, the propagation step can be formulated as [25]:

$$\hat{\mathbf{x}}_{k|k-1} = f(\hat{\mathbf{x}}_{k-1|k-1}, u_k), \quad (16)$$

$$P_{k|k-1} = F_k P_{k-1|k-1} F_k^T + Q_k, \quad (17)$$

where Q_k is the process noise covariance matrix.

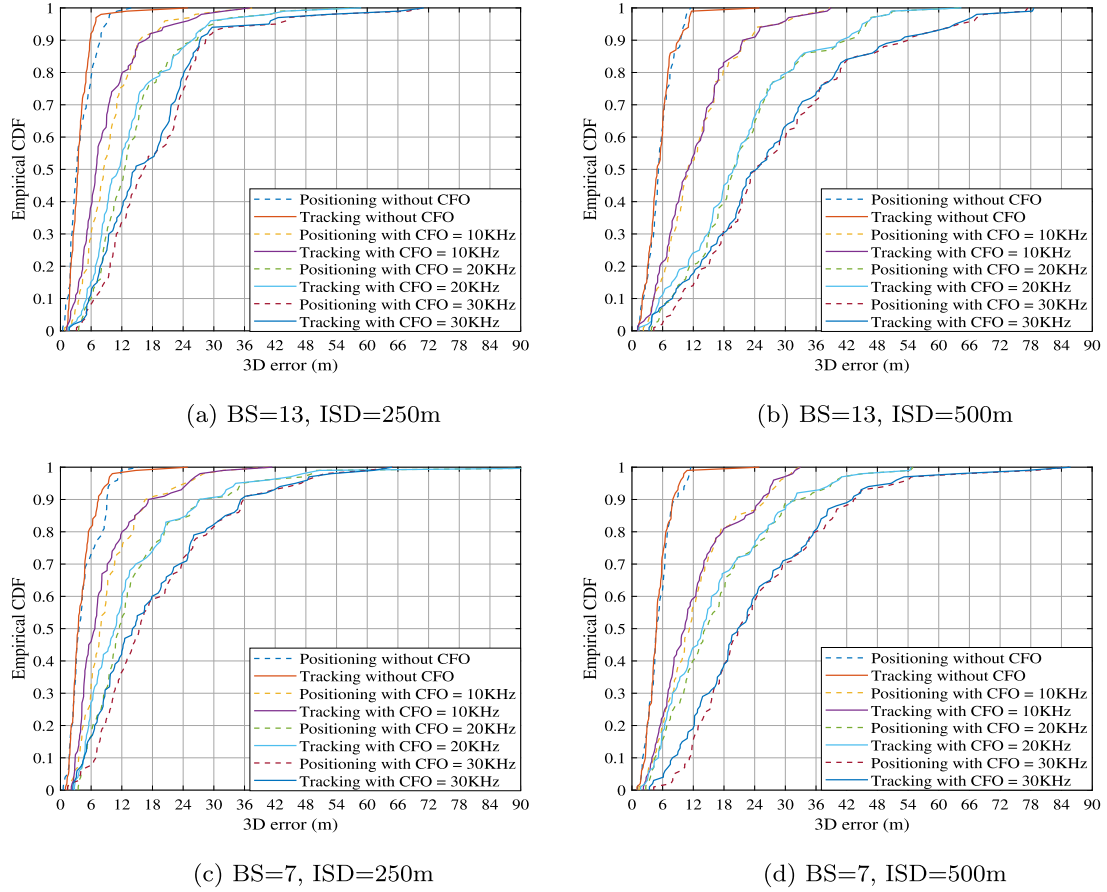


Fig. 11. Impact of CFO on 3D drone localizing and tracking.

Update step

Let K_k represent Kalman gain, $\hat{x}_{k|k}$ be the updated state estimate, and $P_{k|k}$ be the updated error covariance matrix at sampling time k . Then, the update phases of the EKF are provided as follows [25]:

$$K_k = P_{k|k-1} H_k^T (H_k P_{k|k-1} H_k^T + R_k)^{-1}, \quad (18)$$

$$\hat{x}_{k|k} = \hat{x}_{k|k-1} + K_k (z_k - h(\hat{x}_{k|k-1})), \quad (19)$$

$$P_{k|k} = (I - K_k H_k) P_{k|k-1}, \quad (20)$$

where R_k represents the measurement noise. I is the identity matrix.

4. Simulation results and validation

4.1. Simulation setup

The simulation parameters are defined as follows: The simulation setup is configured with 7 and 13 BS receivers, with the ISD between adjacent BS 250 meters and 500 meters. The BS receivers employ a 4X4 URA, positioned at a height of 3 meters. The simulation area covers a square with a dimension of 1000 meters on each side. The drone utilizes a single antenna for transmission, operating with a carrier frequency of 490 MHz and a bandwidth allocation of 1.4 MHz. It sends signal with sampling interval of 0.5 s. In our simulations, the drone follows a spiral trajectory within the x - y plane while hovering at altitudes ranging from 7 to 11 meters, enabling us to analyze its 3D positional estimation performance. For each snapshot along the given trajectory of the drone, the distance to each BS receiver is initially computed, subsequently enabling the determination of the SNR at every BS receiver. In our

simulation, we examine the influence of various impairments on 3D localization and tracking accuracy. We configure the simulation to introduce a CFO ranging from 0 to 30 kHz, PN varying between 0 to 3°, and a BS antenna tilt also within a range of 0 to 3°. The impact of these parameters is then assessed in terms of their effects on the covariance, AOA, and the precision of localization estimations.

4.2. Localization and tracking results

4.2.1. Impacts of CFO

We evaluate the accuracy of 3D localization and tracking, with the simulated results presented in Fig. 11. Doubling the ISD while maintaining the number of BS receivers, Fig. 11(b), the median errors for positioning and tracking are 6 meters without CFO. However, introducing a 30KHz CFO the errors rise to around 24 meters for positioning and tracking. Comparatively, the 90th percentile error increases as the ISD increases and the number of BS decreases. This trend is indicative of the impact of both BS density and ISD on the accuracy of 3D positioning in the presence of CFO. Fig. 11(a) shows that when CFO is not considered, the median errors for positioning and tracking are approximately 3 meters. However, with a 30KHz CFO, these errors increase to approximately 16 meters for positioning and 14 meters for tracking.

4.2.2. Impacts of PN

Fig. 12 shows the influence of PN on 3D drone positioning and tracking for two different ISDs and two BS setups. Notably, for both 13 and 7 BS configurations, as the ISD increases from 250m to 500m, the 3D positioning and tracking errors tend to increase. The 90th percentile values from Fig. 12(a) indicate a positioning error of 7.5 meters without PN and 21 meters with a PN of 3°.

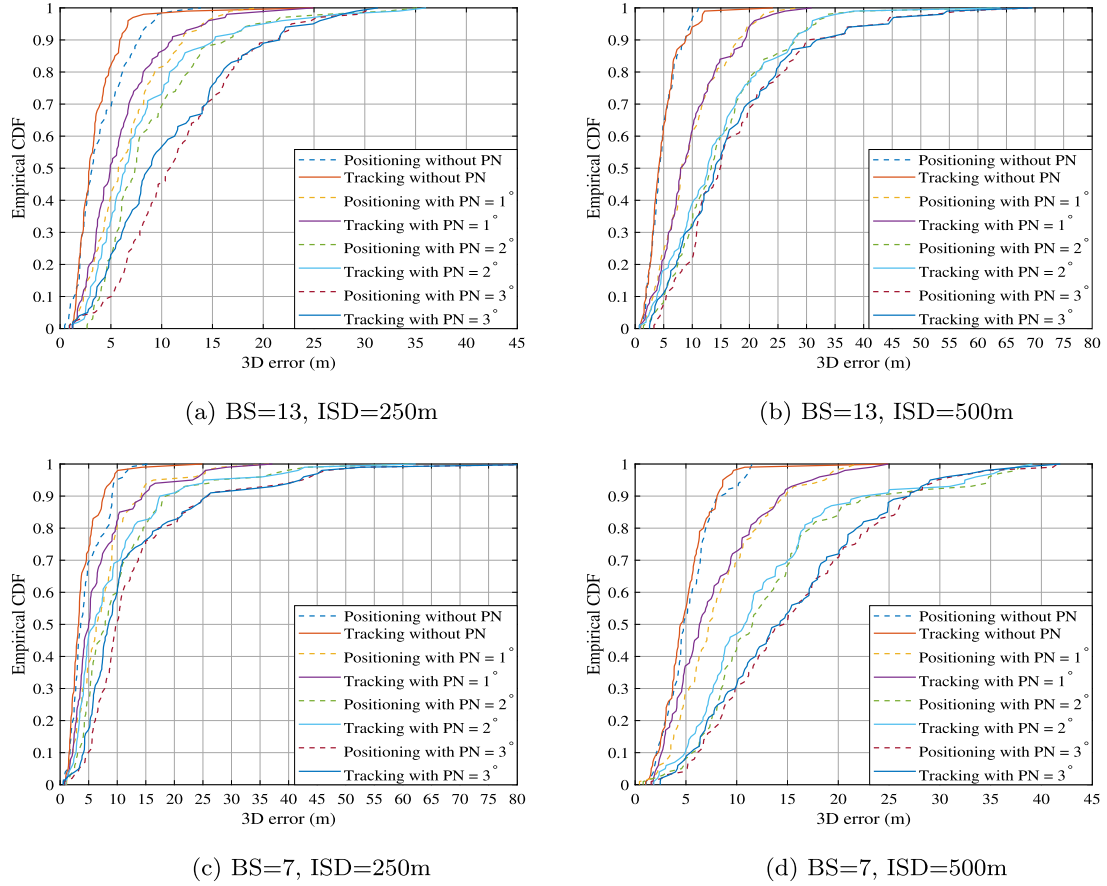


Fig. 12. Impact of PN on 3D drone localizing and tracking.

Table 2
90th Percentile of 3D location (m) error for different impairments.

No. BS	ISD [m]	CFO				PN				Tilting angle			
		0 KHz	10 KHz	20 KHz	30 KHz	0°	1°	2°	3°	0°	1°	2°	3°
13	250	8	17	26	28	7.5	12	17	21	8	11	13	14
	500	10	21	42	54	9	18	27.5	33	10	16	19	24
7	250	10	18	30	36	9	15	20	26	9	12	13	14
	500	10	27	35	43	8	14	22	27	8	12	17	22

Meanwhile, Fig. 12(c) shows a 90th percentile positioning error of 9.5 meters without PN and 26 meters with a PN of 3°. This concludes that for the same ISD, a reduction in the number of BS results in an increase error. For the same area of interest, reducing the number of BS leads to increased errors due to fewer BS providing less diverse angle coverage and fewer measurements. This reduction also stretches each BS's coverage area, heightening susceptibility to signal quality issues like multipath conditions.

4.2.3. Impacts of tilt angle

Fig. 13 highlights the relationship between the down tilt of the BS antenna receiver and its influence on 3D drone localization and tracking for different setups. At the 90th percentile, Fig. 13(a) suggests a positioning error of around 8 meters when the BS antenna is not tilted, increasing to 14 meters with a 3° tilt.

Conversely, Fig. 13(d) demonstrates that increasing the ISD while decreasing the number of BS leads to higher errors at the same percentile, with positioning errors of 9 meters without tilt and 21 meters with a 3° tilt. Essentially, increasing the down tilt of the BS antenna receiver, especially in less dense BS setups, leads to a noticeable drop in drone localization accuracy. Fig. 13 generally shows that the positioning and tracking curves diverge as the tilting angle increases. The

90th percentile of 3D location error under all considered hardware impairments is presented in Table 2.

5. Conclusion

In this paper, we analyze our approach, which employs a spiral trajectory drone equipped with a single antenna for signal transmission, and 4X4 URA receivers positioned at known locations. We examine the impact of CFO, PN, and tilting of BS antenna receivers on AOA-based drone localization and tracking. To validate our methodology, we introduce different PNs and CFOs for each antenna element in the computation of the steering vector at each sampling time. To visualize the impact of these considered impairments on drone localization and tracking, we follow a three-step process in our paper. Firstly, we examine the impact of impairments on the off-diagonal elements of the covariance matrix of the received signal at each BSs. The second step involves visualizing the impact of these impairments on 3D AOA estimation using the MUSIC algorithm for each BS receiver. Finally, having estimated the noisy 3D AOA, we estimate the position of the drone using a LS approach across all the BS receivers, and track the drone using EKF algorithm.

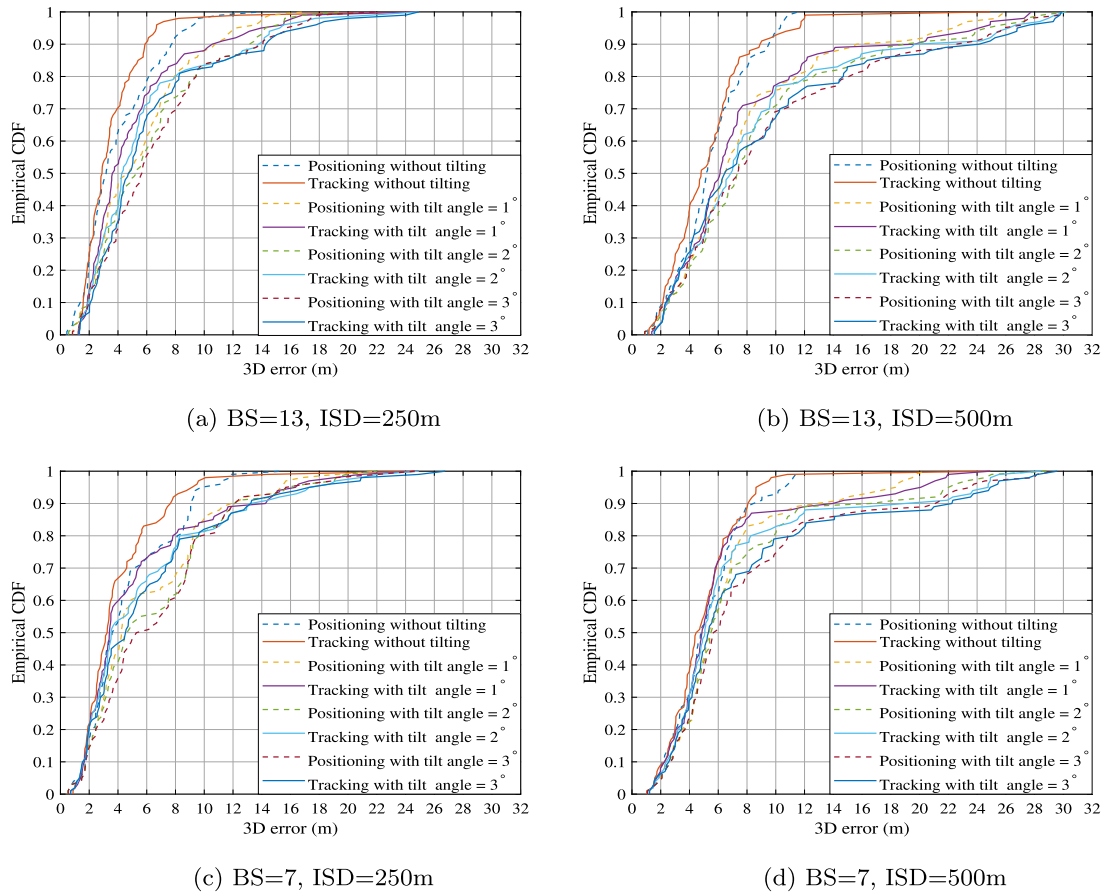


Fig. 13. Impact of down tilt of BS antenna receiver on 3D drone localizing and tracking.

Furthermore, we evaluate and compare the corresponding CRLB for all BSs with the sample variance of the 3D AOA using MUSIC, demonstrating that our results validate the lower bound. Moreover, we investigate how the configuration of the number of BSs and their ISD influences AOA-based drone localization accuracy. Our simulation study reveals that impairments can significantly affect the accuracy of drone location estimation.

CRediT authorship contribution statement

Mehari Meles: Writing – review & editing, Writing – original draft, Visualization, Validation, Software, Methodology, Investigation, Formal analysis, Conceptualization. **Akash Rajasekaran:** Writing – review & editing, Validation, Methodology, Investigation, Conceptualization. **Estifanos Yohannes Menta:** Methodology, Investigation. **Lauri Mela:** Supervision, Software. **Riku Jäntti:** Writing – review & editing, Supervision, Project administration, Funding acquisition, Conceptualization.

Declaration of competing interest

The authors declare that they have no known competing financial interests or personal relationships that could have appeared to influence the work reported in this paper.

Data availability

Data will be made available on request.

References

- [1] Meer IA, Ozger M, Lundmark M, Sung KW, Cavdar C. Ground based sense and avoid system for air traffic management. In: 2019 IEEE 30th annual international symposium on personal, indoor and mobile radio communications. IEEE; 2019, p. 1–6.
- [2] Li Y, Shu F, Shi B, Cheng X, Song Y, Wang J. Enhanced RSS-based UAV localization via trajectory and multi-base stations. *IEEE Commun Lett* 2021;25(6):1881–5.
- [3] Kim T-y, Lee D, Hwang S-s. Cascade AOA estimation technique based on uniform circular array. In: The 9th international conference on smart media and applications. 2020, p. 305–7.
- [4] Weber RJ, Huang Y. Analysis for capon and MUSIC DOA estimation algorithms. In: 2009 IEEE antennas and propagation society international symposium. IEEE; 2009, p. 1–4.
- [5] Qiu X, Wang B, Wang J, Shen Y. AOA-based BLE localization with carrier frequency offset mitigation. In: 2020 IEEE international conference on communications workshops. IEEE; 2020, p. 1–5.
- [6] Broumandan A, Nielsen J, Lachapelle G. Practical results of high resolution AOA estimation by the synthetic array. In: 2008 IEEE 68th vehicular technology conference. IEEE; 2008, p. 1–5.
- [7] Nie W, Han Z-C, Li Y, He W, Xie L-B, Yang X-L, et al. UAV detection and localization based on multi-dimensional signal features. *IEEE Sens J* 2021;22(6):5150–62.
- [8] Wu T, Deng Z, Li Y, Huang Y. Two-dimensional DOA estimation for incoherently distributed sources with uniform rectangular arrays. *Sensors* 2018;18(11):3600.
- [9] Cho H, Liu C, Lee J, Noh T, Quek TQ. Impact of elevated base stations on the ultra-dense networks. *IEEE Commun Lett* 2018;22(6):1268–71.
- [10] Al-Hourani A, Kandeepan S, Lardner S. Optimal LAP altitude for maximum coverage. *IEEE Wirel Commun Lett* 2014;3(6):569–72.
- [11] Kang S, Kim T, Chung W. Hybrid RSS/AOA localization using approximated weighted least square in wireless sensor networks. *Sensors* 2020;20(4):1159.
- [12] Muhammad A. Evaluation of tdoa techniques for position location in cdma systems [Master of Science Thesis], Virginia Polytechnic Institute and State University; 1997.
- [13] Uebayashi S, Shimizu M, Fujiwara T. A study of TDOA positioning using UWB reflected waves. In: 2013 IEEE 78th vehicular technology conference. IEEE; 2013, p. 1–5.

- [14] Nemati M, Baykas T, Choi J. Performance of TDOA and AOA localization techniques for different base-stations topologies. In: 2019 13th international conference on signal processing and communication systems. IEEE; 2019, p. 1–7.
- [15] Chen L, Kishk MA, Alouini M-S. Dedicating cellular infrastructure for aerial users: Advantages and potential impact on ground users. *IEEE Trans Wireless Commun* 2022;22(4):2523–35.
- [16] Meles M, Rajasekaran A, Ruttik K, Virrankoski R, Jäntti R. Measurement based performance evaluation of drone self-localization using AoA of cellular signals. In: 2021 24th international symposium on wireless personal multimedia communications. IEEE; 2021, p. 1–5.
- [17] Meles M, Mela L, Rajasekaran A, Ruttik K, Jäntti R. Drone localization based on 3D-aoa signal measurements. In: 2022 IEEE 95th vehicular technology conference. IEEE; 2022, p. 1–5.
- [18] Meles M, Rajasekaran A, Mela L, Ghazalian R, Ruttik K, Jäntti R. Performance evaluation of measurement based GPS denied 3D drone localization and tracking. In: 2023 IEEE wireless communications and networking conference. IEEE; 2023, p. 1–6.
- [19] Kim S, Kim M. Rotation representations and their conversions. *IEEE Access* 2023;11:6682–99.
- [20] Yuri N, Ilia P. Performance study of beamspace processing DOA estimation by MUSIC and capon methods. In: 2015 international siberian conference on control and communications. IEEE; 2015, p. 1–6.
- [21] Chen Z, Gokeda G, Yu Y. Introduction to direction-of-arrival estimation. Artech House; 2010.
- [22] Menta EY, Malm N, Jäntti R, Ruttik K, Costa M, Leppänen K. On the performance of aoa-based localization in 5G ultra-dense networks. *IEEE Access* 2019;7:33870–80.
- [23] Raol JR, Gopalratnam G, Twala B. Nonlinear filtering: Concepts and engineering applications. CRC Press; 2017.
- [24] Coelho MF, Bousson K, Ahmed K. Survey of nonlinear state estimation in aerospace systems with Gaussian priors. *Adv Aircr Spacecr Sci* 2020;7(6):495.
- [25] Anderson BD, Moore JB. Optimal filtering. Courier Corporation; 2012.